Astron. Astrophys. 335, 1101–1110 (1998)

ASTRONOMY AND ASTROPHYSICS

Particle acceleration efficiency and MHD characteristics of CIR-related shocks

H.-T. Claßen[1], **G. Mann**[1], **and E. Keppler**[2]

[1] Astrophysikalisches Institut Potsdam, An der Sternwarte 16, D-14482 Potsdam, Germany
[2] Max-Planck-Institut für Aeronomie, Postfach 20, D-37191 Katlenburg-Lindau, Germany

Received 15 July 1997 / Accepted 28 April 1998

Abstract. During its southbound journey the Ulysses spacecraft crossed a series of corotating interaction regions (CIRs) building up due to the interaction of fast and slow solar wind streams. We analyse the forward and the reverse shocks marking off the 18 CIR encounters between July 1992 and December 1993. Our investigations look for a correlation between the particle acceleration efficiency expressed by the particle flux measured at the time of shock crossing and the MHD characteristics of the shocks; i.e., Alfven-Mach number (M_{A1}), density and magnetic field compression ratios (r_N, r_B), and the angle between shock normal and upstream magnetic field (θ_{Bn}). The results of this analysis show that the highest fluxes of 300 keV electrons and 1 MeV protons are observed when the conditions $M_{A1} > 2.5$ and $50° \leq \theta_{Bn} \leq 75°$ are simultaneously fulfilled by the shocks. These investigations are supplemented by a computation of the first critical Alfven-Mach number for typical parameters of CIR-related shocks. Furthermore, we discuss possible acceleration mechanisms by an analysis of the spectral indices of protons and Helium.

Key words: solar wind – interplanetary medium – acceleration of particles – shock waves

1. Introduction

Collisionless shock waves can be generated by different processes in the heliosphere. In the solar corona shock waves appear either as blast waves or as piston driven shocks (Parker 1961). In most cases, the shock waves observed in the interplanetary medium are piston driven; e.g., bow shocks and travelling interplanetary shocks (Hundhausen 1972, Russell 1985). Furthermore, the development of shocks at the interaction region of high- and low-speed streams is a well-known feature of the evolution of streams for increasing heliocentric distances (Smith & Wolfe 1976, Gosling et al. 1976, Gosling 1996).

From a magnetohydrodynamical point of view, all of these shocks can be characterized by a few dimensionless parameters taken from the one-fluid description of plasmas; i.e., the Alfven-Mach number $M_{A1} = u_1/V_{A1}$ as the ratio of the upstream flow velocity u_1 and the Alfven velocity $V_{A1} = B_1/(\mu_0 m_p N_1)^{1/2}$, the upstream plasma beta $\beta_1 = N_1 k_B T_1/(B_1^2/2\mu_0)$ as the ratio of thermal and magnetic pressure, and the angle θ_{Bn} between the shock normal and the upstream magnetic field. B_1, N_1, and T_1 denote the upstream magnetic field strength, particle number density, and temperature, while the constants μ_0, m_p, and k_B are the permeability of free space, the proton mass, and the Boltzmann constant, respectively. After fixing these initial conditions, the downstream state of the plasma (denoted by index 2) can be computed using the conservation of mass, momentum, and energy flow at the shock (e.g., Tidmann & Krall 1971, Priest 1982). Therefore, the density compression $r_N = N_2/N_1$, the magnetic field compression $r_B = B_2/B_1$, and the temperature jump $r_T = T_2/T_1$ are functions of M_{A1}, β_1, and θ_{Bn} described by the so-called jump- or Rankine-Hugoniot conditions. Furthermore, the Rankine-Hugoniot conditions contain the adiabatic index κ as a parameter.

Assuming a scalar resistivity as the only dissipation mechanism at MHD shocks, the Rankine-Hugoniot conditions cannot be satisfied for shocks above a certain critical Alfven-Mach number (Kantrowitz & Petschek 1966, Edmiston & Kennel 1984). This threshold velocity - the first critical Mach number - at which resistivity fails to steepen the shock is reached when the downstream velocity parallel to the shock normal is equal to the downstream sound speed; i.e., $u_{2n} = c_{s2}$. With the addition of viscous dissipation to the fluid model the jump conditions can again be satisfied but the shock is structured with two different length scales for the different dissipation mechanisms (e.g., Kennel et al. 1985). The critical Alfven-Mach number M_{A1}^* and the associated critical magnetic field jump r_B^* are functions of β_1 and θ_{Bn}. The different behaviour of the magnetic field at sub- and supercritical shock waves was investigated by in-situ measurements at the earth's bow shock (e.g., Mellot 1985).

Furthermore, various satellite missions showed that collisionless shocks not only transform the kinetic energy of the upstream plasma flow into heat, but they are also very efficient particle accelerators. Thus, at the earth's bow shock roughly 15% of the solar wind energy goes into superthermal particles (Ellison et al. 1990). The theories for the acceleration of charged particles at shock waves contain two basic ingredients, a deterministic, time-reversible shock-drift acceleration (see Armstrong et al. 1985, for a review) and a stochastical diffusive shock

Send offprint requests to: H.-T. Claßen

acceleration (see Scholer 1985, for a review), generally called first-order Fermi process (Fermi 1949). Both theories have been developed to very sophisticated levels, where the pure form of shock-drift acceleration, i.e., the particles experience just a single shock encounter, is most efficient at nearly perpendicular shocks ($\theta_{Bn} \approx 90°$). The first-order Fermi process is adopted for quasi-parallel shocks ($0° \leq \theta_{Bn} \leq 45°$). The major problems connected with these theories are the question of electron acceleration and possible seed populations of pre-accelerated particles injected into the acceleration process.

The aim of our paper is to find a correlation between the MHD characteristics (e.g., M_{A1} and θ_{Bn}) of CIR-related shock waves and the efficiency of particle acceleration at these shocks. In the past, investigations mostly refer to piston driven travelling interplanetary shock waves near 1 AU (e.g., van Nes et al. 1984). As it has been done in that study we will take the particle flux of high energy particles at the time of shock crossing as a measure for the particle acceleration efficiency. Thus, we will concentrate on both electrons in the energy range 100–400 keV and protons in the range 0.8–1.0 MeV. The data for our analysis are taken from various experiments from the Ulysses spacecraft and cover the southbound passage from July 1992 to December 1993. These observations are briefly described in the next section. The data analysis is presented in Sect. 3, where we first compute the Alfven-Mach numbers of the CIR-related shocks according to a best fit to the measured density and magnetic field jump. The computed Alfven-Mach numbers are compared with the measured fast Mach numbers. In a next step we determine the magnetic field jump for critical shocks and use this field jump to decide which of the CIR shocks are sub- and supercritical, respectively. Finally, we present the results for the correlation between particle peak flux and θ_{Bn} and the Alfven-Mach number M_{A1}. Furthermore, we discuss possible acceleration mechanisms, i.e., a first-order Fermi process and shock-drift acceleration. In Sect. 4 we briefly check the validity of the MHD description of CIR-related shock waves and compare the results of our data analysis concerning acceleration efficiency at CIR shocks with measurements at travelling interplanetary shocks and with the predictions of computer simulations of the different acceleration processes.

2. Observations

The plasma data of CIR-related shock waves are taken from the common data pool of the Ulysses spacecraft mission. The time of crossing the CIR forward and reverse shocks, the angle θ_{Bn}, and the magnetic field jump r_B are adopted from Balogh et al. (1995). The numbering of the CIRs is in accordance with Bame et al. (1993). During this time interval Ulysses moved from 5.34 to 4.28 AU in radial distance and climbed down from $-13.19°$ to $-39.61°$ in heliographic latitude. The plasma- and magnetometer data of the shocks are measurements of the Ulysses solar wind plasma experiment (SWOOPS, Bame et al. 1992) and the Vector Helium and Fluxgate Magnetometers (VHM/FGM, Balogh et al. 1992). In order to determine the magnetic field strength $B_{1(2)}$, the particle number density $N_{1(2)}$ and the temperature $T_{1(2)}$ in the upstream (downstream) region, we took averages over 10 minutes for the magnetic field and 90 minute averages for the plasma data. The results for the upstream plasma state are shown in columns 3, 5, and 7 of the CIRs listed in Table 1. The corresponding jump of these parameters are shown in columns 4, 6, and 8. The error limits are the standard deviations taken from data with a shorter time averaging; i.e., 3 minutes for B and 30 minutes for N and T, taking into account also the neighbouring time intervals. The upstream plasma beta β_1 was computed according to

$$\beta_1 = \frac{N_1 k_B T_1}{B_1^2/(2\mu_0)}\,, \tag{1}$$

where the error for the plasma beta was evaluated due to error propagation in N_1, T_1, and B_1.

The particle data used in columns 12–15 were taken from the Ulysses-EPAC experiment (Keppler et al. 1992). The particle fluxes j_e and j_p at the time of shock crossing are omnidirectional, 60 minutes-averaged fluxes from the electron and proton channels between 100–380 keV and 768–990 keV, respectively. γ_p denotes the mean downstream spectral index (including standard deviation) for protons in the energy range between 508 and 1559 keV. γ_{He} is the spectral index for Helium immediately downstream of the shock crossing in the energy range 0.4–4 MeV/nucleon. The proton and Helium spectra used 60 and 120 minutes-averaged data, respectively. The flux ratio p/He was calculated from 60 minutes-averaged proton and Helium fluxes with nearly the same energy range; i.e., 629–768 keV for protons and 713–804 keV/nucleon for Helium. An analysis of the spectral index for electrons is not included in the present study since the Ulysses-EPAC experiment measures only electrons in two spin averaged channels ($0.1 < E < 0.38$ MeV and $E > 0.18$ MeV).

The column labeled θ_{Bn} contains the angle between the shock normal and the upstream magnetic field direction taken from Balogh et al. (1995); the uncertainty range has been omitted but can be found in that paper. The "$\perp$" and "$\parallel$" signs indicate whether the shock is a quasi-perpendicular or quasi-parallel shock; i.e., $45° \leq \theta_{Bn} < 90°$ or $0° \leq \theta_{Bn} < 45°$. The "$+$" and "$-$" signs refer to super- and subcritical shocks with respect to the first critical Alfven-Mach number. These calculations are analysed in the next section in connection with the determination of the Alfven-Mach number M_{A1} according to the Rankine-Hugoniot relations (cf. Table 1, column 11).

3. Data analysis

The Rankine-Hugoniot relations are based on the conservation of mass, momentum and energy flow across the shock surface. Assuming a Maxwellian particle distribution in the up- and downstream region and equal temperatures for all charged particles, they achieve their simplest description in the so-called de Hoffmann-Teller frame (e.g., Priest 1982). This special frame of reference is chosen in such way that the plasma flow speed is directed parallel to the magnetic field in both up- and downstream regions; i.e., the electric field is removed in these regions

Table 1. Summary of the properties of 18 CIR-related shock-pairs observed by Ulysses.

No	Date	B_1 [nT]	B_2 / B_1 (Ba, 95)	N_1 [cm^{-3}]	N_2 / N_1	T_1 [10^5K]	T_2 / T_1	θ_{Bn}	β_1	M_{A1} (RH)	j_e | j_p [par./cm^2 srMeV/N]	γ_p	γ_{He}	p/He
1 F	1992 185	0.70±0.05	1.70±0.14	0.25±0.05	1.4±0.3	0.20±0.03	1.5±0.3	54° ⊥/∥-/+	0.35±0.18	1.6±0.3	100 | 10	2.18±0.24	2.52	11±2
1 R	1992 188	0.65±0.05	1.73±0.06	0.16±0.03	1.7±0.3	0.40±0.05	1.4±0.3	77° ⊥ -/+	0.52±0.24	1.9±0.2	0 | 2	2.47±0.60	3.66	20±5
2 F	1992 202	0.75±0.05	2.17±0.15	0.33±0.07	2.3±0.2	0.15±0.07	2.7±0.8	59° ⊥ +/-	0.31±0.25	2.2±0.5	0 | 20	3.82±0.34	3.81	32±4
2 R	1992 205	0.55±0.06	1.90±0.17	0.15±0.05	3.1±0.9	0.20±0.04	2.5±0.5	20° ∥ +/-	0.34±0.25	2.7±0.5	0 | 1	3.42±0.10	3.71	15±2
3 F_1	1992 226	1.20±0.05	1.21±0.01					67° ⊥			5 | 20	1.57±0.31	1.83	40±2
3 F_2	1992 229	2.10±0.05	1.11±0.01	0.32±0.02	1.25±0.15	0.40±0.05	1.1±0.1	73° ⊥ -	0.10±0.03	1.3±0.2	0 | 15	2.25±0.46	2.54	32±2
3 R_2	1992 233	1.20±0.03	1.59±0.13	0.35±0.05	1.4±0.3	1.0±0.1	1.4±0.2	52° ⊥ -/+	0.84±0.25	1.5±0.3	15 | 40	1.29±0.42	1.61	4±1
3 R_1	1992 234	0.70±0.03	1.62±0.10	0.15±0.05	1.7±0.3	0.6±0.1	1.7±0.1	43° ⊥/∥-/+	0.64±0.35	1.8±0.2	30 | 25	1.49±0.43	2.15	5±1
4F	1992 257	3.0±0.5	1.44±0.09	0.6±0.1	1.7±0.6	1.75±0.15	1.9±0.1	51° ⊥/∥ -	0.40±0.23	1.6±0.1	230 | 600	1.79±0.22	2.00	16±2
4R	1992 259	0.45±0.03	3.73±0.84	0.05±0.01	2.6±0.6	0.5±0.02	3.8±0.2	64° ⊥ +	0.43±0.16	5.3±2.6	60 | 30	1.85±0.24	1.77	15±2
5 F	1992 282	1.50±0.25	1.35±0.05	0.60±0.10	1.4±0.3	0.25±0.09	1.7±0.9	75° ⊥ -	0.23±0.20	1.42±0.5	30 | 20	2.47±0.61	2.75	35±2
5 R	1992 285	0.50±0.10	2.46±0.23	0.12±0.04	2.3±0.4	0.50±0.15	3.0±1.0	68° ⊥ +	0.83±0.51	3.00±0.5	80 | 200	1.67±0.36	2.05	4±2
6 F	1992 307	0.50±0.25	1.88±0.09	0.10±0.05	3.1±1.0	0.20±0.10	4.0±1.0	82° ⊥ -	0.28±0.20	2.37±0.5	300 | 150	2.88±0.18	3.17	22±4
6 R	1992 310	0.80±0.20	2.60±0.50	0.27±0.07	2.2±0.3	0.80±0.30	1.9±0.6	+	1.17±0.70		900 | 400	1.59±0.26	1.97	6±1
7F	1992 334	0.51±0.11	1.83±0.14	0.09±0.02	3.3±0.8	0.10±0.03	5.0±2.0	42°∥/⊥ +/-	0.82±0.70	2.97±0.5	5 | 50	2.87±0.21	2.89	15±3
7 R	1992 336	0.40±0.20	3.00±1.00	0.05±0.02	3.0±0.5	0.50±0.20	3.3±1.0	RW +	0.54±0.40		180 | 800	1.26±0.20	2.16	4±1

columns 3–10: Plasma data, with magnetic field strength B, particle number density N, temperature T, angle between upstream magnetic field and shock normal θ_{Bn}, plasma beta β, Alfven-Mach number M_A. Indices 1 and 2 refer to the up- and downstream region, respectively.
columns 11–15: Characteristic data for energetic charged particles, particle fluxes for 0.1–0.4 MeV electrons j_e and 0.8–1.0 MeV proton j_p at the time of shock crossing (the exclamation marks indicate shocks with preceding interplanetary shocks or solar energetic particle events); downstream spectral indices for protons $\gamma_{\rm p}$ and Helium $\gamma_{\rm He}$. p/He denotes the flux ratio of protons to Helium at the time of shock crossing.

(de Hoffmann & Teller 1950). The transformation between the shock rest frame (superscript R) and the de Hoffmann-Teller frame (superscript HT) is given by $\boldsymbol{v}^{HT} = \boldsymbol{v}^R + \boldsymbol{v}_{HT}$, with (Landau & Lifshitz 1957)

$$\boldsymbol{v}_{HT} = \frac{\boldsymbol{n} \times (\boldsymbol{u}_1^R \times \boldsymbol{b}_1)}{\boldsymbol{n} \cdot \boldsymbol{b}_1}\,, \tag{2}$$

$\boldsymbol{n}$ and $\boldsymbol{b}_1$ denoting the shock normal and the normal vector in the direction of the upstream magnetic field. For $\boldsymbol{u}_1^R \| \boldsymbol{n}$, the magnitude of the de Hoffmann-Teller velocity is $v_{HT} = u_1^R \tan\theta_{Bn}$, while the magnitude of $\boldsymbol{v}_{HT}$ for an oblique plasma flow contains also trigonometric functions of θ_{Vn} describing the angle between the shock normal and the direction of the upstream plasma flow speed. Since this angle cannot be obtained from our previous data set (see Sect. 2) we will assume $\boldsymbol{u}_1^R \| \boldsymbol{n}$ for the further analysis.

In the de Hoffmann-Teller frame the density jump across the shock r_N can be computed via (Priest 1982)

$$\begin{aligned}(m_{A1}^2 \;-\; & r_N)^2\{\kappa\beta_1 r_N \\ & +\; m_{A1}^2\cos^2\theta_{Bn}[(\kappa-1)r_N-(\kappa+1)]\} \\ & +\; m_{A1}^2 r_N \sin^2\theta_{Bn}\{[\kappa+(2-\kappa)r_N]m_{A1}^2 \\ & -\; r_N[(\kappa+1)-r_N(\kappa-1)]\} = 0\,,\end{aligned} \tag{3}$$

with $m_{A1} = u_1^{HT}/V_A$. For fast MHD shocks the magnetic field compression obeys $r_B > 1$ and is given by

$$r_B = \left\{\cos^2\theta_{Bn} + \frac{(m_{A1}^2-1)^2}{(m_{A1}^2-r_N)^2} r_N^2 \sin^2\theta_{Bn}\right\}^{1/2}\,. \tag{4}$$

Transforming back into the shock rest frame r_N and r_B are unchanged to the order $O((v_{HT}/c)^2)$. For the analysed CIR shocks from Table 1 this correction is negligible since the largest angle θ_{Bn} is $82°$ resulting in $v_{HT} \approx \tan 82° \cdot 100\,\mathrm{km/s} = 0.002c$. Furthermore, the transformation of the Alfven-Mach number from the de Hoffmann-Teller frame (m_{A1}) to the shock rest frame (M_{A1}) is given by $M_{A1} = u_1^R/V_A = m_{A1}\cos\theta_{Bn}$.

Table 1. (continued)

No	Date	B_1 [nT]	B_2 / B_1 (Ba, 95)	N_1 [cm^{-3}]	N_2 / N_1	T_1 [10^5K]	T_2 / T_1	θ_{Bn}	β_1	M_A (RH)	j_e | j_p [par./cm^2 srMeV/N]	γ_p	γ_{He}	p/He
8F	1992 361	0.75±0.15	1.56±0.10	0.18±0.03	2.0±0.5	0.20±0.10	2.5±0.5	25° ∥ -	0.22±0.20	1.7±0.5	10 | 70	2.93±0.22	3.59	35±8
8 R	1992 364	0.70±0.20	2.45±0.27	0.10±0.05	2.2±0.9	0.50±0.10	4.4±0.5	70° ⊥ +/-	0.35±0.30	2.74±0.5	100 | 200	2.74±0.18	2.57	17±2
9F	1993 020	1.00±0.25	1.57±0.05	0.80±0.30	2.0±0.6	0.75±0.25	2.0±0.7	72° ⊥ -	2.08±1.02	2.47±0.5	10 | 40	2.96±0.41	3.48	20±3
9 R	1993 022	0.75±0.25	2.94±0.11	0.20±0.05	2.4±0.8	0.80±0.10	3.7±1.0	69° ⊥ +	0.99±0.50	4.33±0.8	500 | 300	1.56±0.22	1.83	5±1
10F	1993 051	0.55±0.02	1.14±0.05	0.07±0.02	1.9±0.5	0.22±0.01	1.5±0.1	28° ∥ -	0.18±0.07	1.2±0.1	0 | 30	2.96±0.30	2.71	15±3
10R	1993 053	0.70±0.05	2.73±0.09	0.14±0.02	2.5±0.3	0.45±0.05	4.4±0.4	72° ⊥ +	0.45±0.18	3.0±0.4	10 | 100	2.90±0.13	2.92	8±1
11F	1993 076	0.55±0.03	1.73±0.13	0.24±0.02	1.7±0.2	0.23±0.03	1.5±0.4	42°∥/⊥+/ -	0.65±0.21	1.9±0.2	10 | 80	2.23±0.07	2.92	14±1
11R	1993 079	0.85±0.08	1.63±0.05	0.25±0.05	1.6±0.3	1.9±0.1	1.2±0.1	57° ⊥ +/ -	2.3±1.0	2.4±0.3	20 | 50	2.39±0.07	2.29	10±2
12R	1993 105	1.70±0.05	1.66±0.19	0.20±0.03	1.4±0.25	2.0±0.2	1.2±0.1	29°∥/⊥+/ -	0.48±0.15	1.6±0.2	0 | 10	3.55±0.16	3.52	13±1
13 R	1993 130	1.00±0.20	2.07±0.19	0.20±0.03	2.5±0.4	2.0±0.2	1.5±0.6	59° ⊥ +	1.38±0.70	3.1±0.5	50 | 300	2.17±0.35	2.66	10±1
14 R	1993 156	0.80±0.05	1.99±0.24	0.20±0.05	1.75±0.3	2.1±0.3	1.5±0.5	36° ∥/ ⊥ +	2.27±1.17	3.0±0.6	0 | 30	3.07±0.18	3.03	12±1
15 F	1993 180	0.80±0.05	2.20±0.10	0.18±0.03	1.72±0.4	1.0±0.2	1.8±0.3	65° ⊥ +	0.98±0.48	2.7±0.4	70 | 70	2.97±0.15	2.78	70±5
15 R	1993 183	0.90±0.10	2.29±0.18	0.15±0.03	1.5±0.5	1.8±0.1	1.7±0.1	19 ° ∥ +	1.16±0.55	2.8±1.0	50 | 50	2.42±0.16	2.11	8±2
16 R	1993 207	0.75±0.15	2.09±0.25	0.20±0.04	2.0±0.5	0.8±0.2	2.7±0.8	39°∥/⊥ +/-	0.99±0.68	3.1±0.5	0 | 30	4.23±0.24	4.88	35±5
17 R	1993 244	0.40±0.05	1.50±0.08					46° ⊥/ ∥			0 | 0			
18 R	1993 261	0.90±0.20	1.77±0.36	0.90±0.20	1.5±0.3	0.90±0.20	1.8±0.3	65° ⊥ -/+	1.15±0.50	2.11	0 | 7	2.52±0.79	3.56	10±2

The Alfven-Mach number M_{A1} in column 11 from Table 1 was computed in the following way. Starting in the de Hoffmann-Teller frame we took the plasma beta needed in Eqs. 3 and 4 from Table 1 and choose an adiabatic index $\kappa = 5/3$. This value for the ratio of specific heats seems to be appropriate, at least for interplanetary shock waves (Russell et al. 1983). Then, we computed the density and magnetic field jumps according to Eqs. 3 and 4 for increasing values of the Alfven-Mach number m_{A1}. Finally, we chose the Alfven-Mach number m_{A1} producing the least mean square fit to the measured density and magnetic field jumps (r_N and r_B). Thus, the Alfven-Mach number from Table 1 is essentially this Mach number transformed back into the shock rest frame. The relation between the measured fast Mach number M_f in the paper by Balogh et al. (1995) and M_{A1} is given by

$$M_f = u_1^R/c_{f1} = \sqrt{2}M_{A1} \left[(\kappa\beta_1/2+1) + \sqrt{(\kappa\beta_1/2+1)^2 - 2\kappa\beta_1\cos^2\theta_{Bn}}\right]^{-1/2} . \quad (5)$$

Comparing the Alfven-Mach numbers computed according to the Rankine-Hugoniot relations with the measured fast Mach numbers we find an agreement of 74% within the computed error ranges. This result is very good if we keep in mind, that the measured Mach numbers in Balogh et al. (1995) are only rough estimations (according to the authors) and are given without uncertainty range. Furthermore, it should be emphasized that nearly all reverse shocks are faster than the corresponding forward ones.

Comparing this result with the fluxes of high energy particles, which are in most cases higher for the reverse shocks, we evaluated the first critical Alfven-Mach number. As already mentioned in the Sect. 1, this Mach number is reached when $\boldsymbol{u_2}\cdot\boldsymbol{n} = c_{s2}$ (Edmiston & Kennel 1984). Since the downstream values of plasma flow and sound speed are determined by the upstream conditions, the aforementioned equation enables us to compute the first critical Alfven-Mach number. In the de Hoffmann-Teller frame the implicit definition of this number reads explicitly

$$(m_{A1}^4 - 2m_{A1}^2 r_N + r_N^2) [(\kappa+1)m_{A1}^2\cos^2\theta_{Bn} - \kappa\beta_1 r_N^2 - (\kappa-1)m_{A1}^2 r_N^2] + (\kappa-1)(m_{A1}^6 - 2m_{A1}^4 + m_{A1}^2)r_N^2\sin^2\theta_{Bn} = 0\,. \quad (6)$$

Thus, the first critical Alfven-Mach number can be obtained solving Eqs. 3 and 6. This results in a function of θ_{Bn} and β_1. Keeping in mind the uncertainties concerning the Mach numbers, it is more convenient to compute the critical magnetic field jump. This can easily be done by evaluating r_B (Eq. 4) for the

critical Mach number. Doing so we eliminate several problems: On the one hand, the magnetic field jump has the same value for the de Hoffmann-Teller and the shock rest frame and on the other hand the relative error for r_B is smaller than the relative error in M_{A1}. The results of this analysis are shown in Fig. 1. This figure shows the computation of the critical magnetic field jump for three different values of the upstream plasma beta as solid ($\beta_1 = 1$), dashed ($\beta_1 = 0.5$), and dotted ($\beta_1 = 0.05$) lines as a function of θ_{Bn}. Furthermore, the figure contains the measured values of θ_{Bn} and r_B from Table 1, distinguishing between forward (Fig. 1a) and reverse shocks (Fig. 1b). As a first result it can be seen that the magnetic field jumps for reverse shocks are higher than the jumps at forward shocks. Furthermore, taking into account that the field jump for fixed values of θ_{Bn} and β_1 increases with increasing Mach number, Fig. 1 provides the possibility to decide which of the shocks are super- and subcritical shocks, respectively. Therefore, we have to look into the data from Table 1, select the plasma beta, and determine whether the shock lies above or below the corresponding plasma beta line for the critical magnetic field jump. If the data point marking the individual shock lies above (below) this line the shock is supercritical (subcritical). This was done in the θ_{Bn}–column from Table 1 marked by the "$+$" and "$-$" signs. As can be seen from Fig. 1, the greatest uncertainties arise from an exact determination of θ_{Bn}. Thus, it is uncertain for some shocks whether they are either sub/supercritical or quasi-parallel/perpendicular. These situations are labeled "$-/+$" or "$\parallel$ / $\perp$", where the first sign specifies the most probable case.

Additional information included in Fig. 1 concerns the particle acceleration efficiency at the individual shocks. The solid up or down triangles belong to those shocks with a particle flux of $1\,\mathrm{MeV}$ protons larger than $50\,\mathrm{particles}/(\mathrm{cm}^2\mathrm{srMeV})$ at the time of shock crossing. This shows that the shocks with the highest fluxes of accelerated particles are very likely supercritical.

A more detailed analysis of the correlation between the MHD parameters of the CIR shocks and the particle acceleration efficiency was carried out in Figs. 2 and 3. Fig. 2 shows the particle flux of 100–300 keV electrons (open circles) and 1 MeV protons (filled circles) plotted against Alfven-Mach number (Fig. 2a) and the angle θ_{Bn} (Fig. 2b). In this context it should be mentioned that the 60 minute-averages used for this analysis were taken from a continuous determination of the particle flux so that the the shock transition time does not necessarily halve the averaging interval. Due to this method the results might be biased as long as exact numbers for the particle flux are required. On the other hand these restrictions are not crucial in the present context since the averaging interval is relatively short. Thus, we find that at first glance the correlation between these MHD parameters and particle flux is rather poor, just showing the possibility of increasing the peak flux with increasing Mach number (Fig. 2a) and that the most efficient particle accelerating shocks seem to be quasi-perpendicular; i.e., $\theta_{Bn} \geq 45°$ (Fig. 2b). But there are always CIR shocks with high Mach number or with quasi-perpendicular shock geometry with low fluxes of accelerated particles.

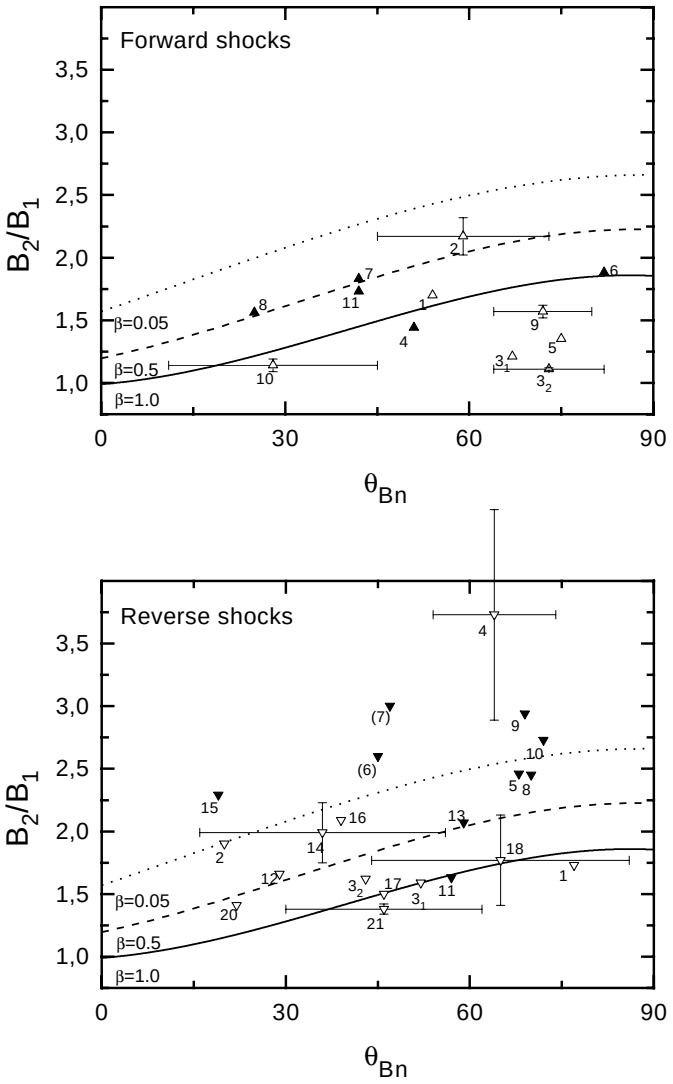

Fig. 1a and b. Measured magnetic field jump and computed critical magnetic field jump for forward (**a**) and reverse shocks (**b**), respectively. The measured values for B_2/B_1 and θ_{Bn} were taken from Balogh et al. (1995). The dotted, dashed, and solid curves are theoretical computations according to Eqs. 3 and 6 for a upstream plasma beta of 0.05, 0.5, and 1.0, respectively. The filled up and down triangles indicate those shocks with a proton flux greater than 50 part./$(\mathrm{cm}^2\mathrm{srMeV})$.

The relationship becomes plain if we consider two-dimensional plots of particles peak fluxes against θ_{Bn} and M_{A1} (Fig. 3). Fig. 3a shows the correlation between the proton fluxes and these two parameters. From this representation it can be seen that the quasi-perpendicular shocks from Fig. 2b with low acceleration rates are very slowly moving shocks. Thus, Fig. 3a shows that the shocks with the highest proton fluxes at the time of shock crossing are those with $M_{A1} > 2.5$ and $50° < \theta_{Bn} < 75°$. This rather severe condition becomes weakened if we change to the electron data (Fig. 3b). In this case we also find high flux rates for relatively slow shocks (e.g., 4F) or for quasi-parallel shocks (e.g., 15R). We will return to this point in the next section in

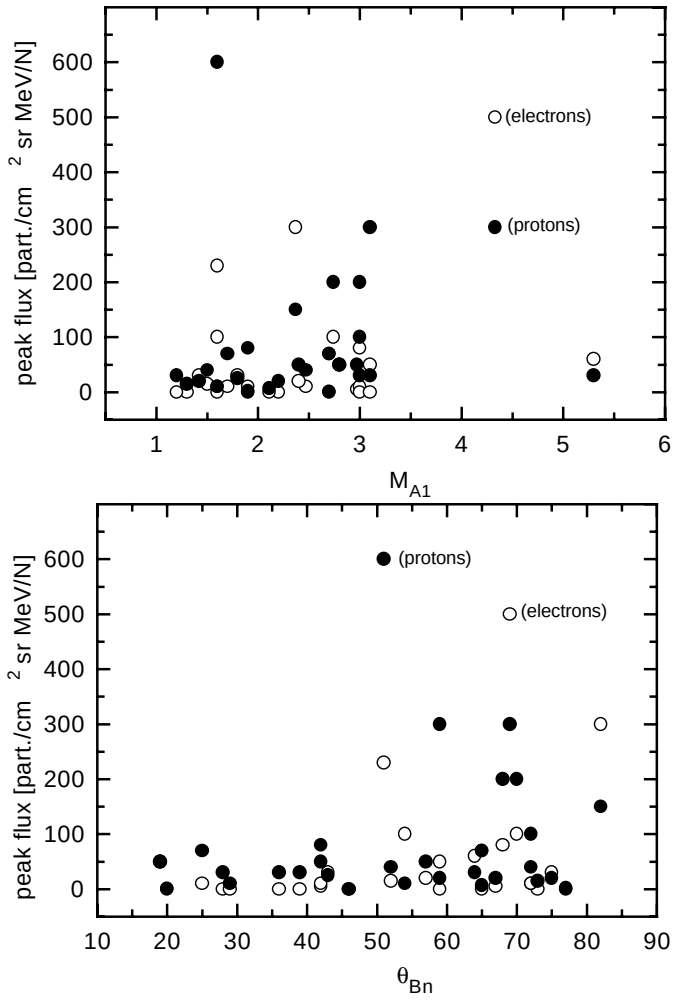

Fig. 2a and b. One parametrical correlation between particle flux and computed Alfven-Mach number (**a**) and shock geometry (**b**). The open and filled circles denote the electron and proton fluxes according to Table 1.

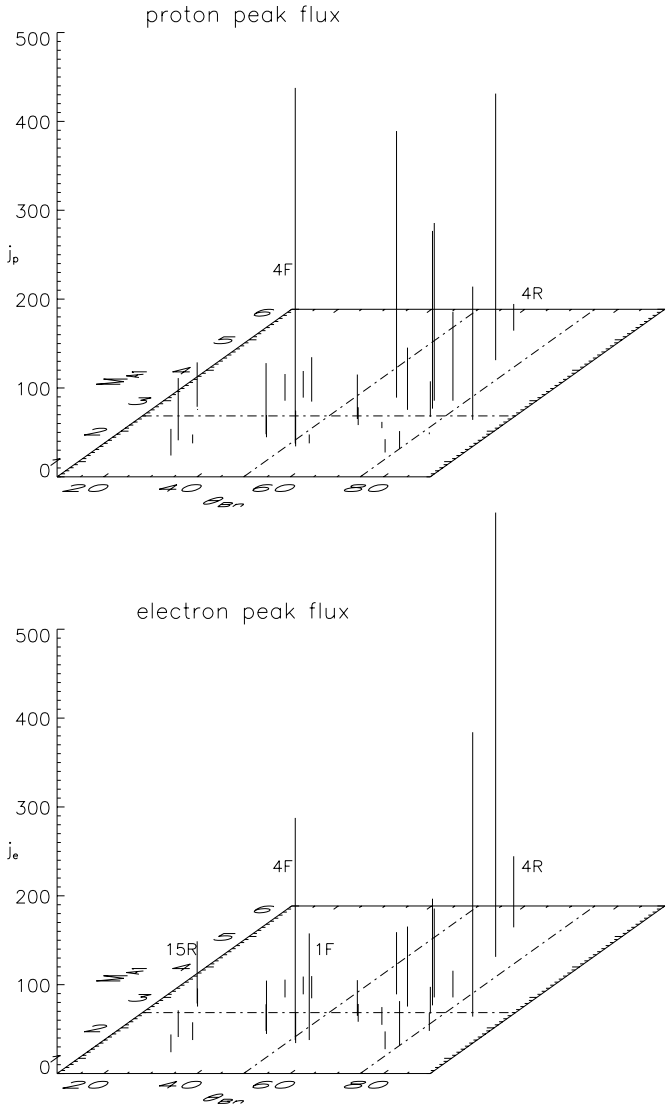

Fig. 3a and b. Two parametrical correlation between particle flux and θ_{Bn}–M_{A1} variation. **a** 0.8–1.0 MeV proton flux and **b** 0.1–0.4 MeV electron flux at the time of shock crossing. The dashed-dotted lines separate regions with high and low particle acceleration efficiency.

connection with the discussion of pre-acceleration processes and seed particles.

Furthermore, Table 1 contains information about the spectral indices of protons γ_p and Helium γ_{He} in the energy range between roughly 0.5–1.5 MeV/nucleon. The relations between γ_p and the density jump $r_N = N_2/N_1$ and γ_p and γ_{He} are presented in Fig. 4a and b, respectively. Again, in both figures the filled circles denote shocks with $j_p > 50\,\mathrm{particles/(cm^2 sr MeV)}$. While Fig. 4a shows only a weak interdependence between density compression and γ_p with no clear functional relationship, it is obvious from Fig. 4b that there is a relation between the spectral indices of the ions under consideration. The straight in this line shows the best linear fit for linear regression (for all data points) according to

$$\gamma_{\mathrm{He}} = a + b\gamma_p\,, \tag{7}$$

with $a = 0.63$ and $b = 0.78$. The correlation coefficient is $r = 0.89$ giving a probability of $p = 2.53 \cdot 10^{-11}$ for a random distribution.

If we assume a particle acceleration by a first-order Fermi process the spectral index $\gamma_{1\mathrm{st}}$ should be related to the density compression across the shocks r_N according to $\gamma_{1\mathrm{st}} = (r_N+2)/(2r_N-2)$ (Axford et al. 1977, Blandford & Ostricker 1978). This relationship is shown in Fig. 4a with the dashed line, the dotted lines indicate an uncertainty range of 30%. According to this range nearly all shocks with a sufficient high particle flux lie in this area, although the functional relationship is not clearly recognizable. Furthermore, the simplest form of diffusive shock acceleration predicts no differences between proton and ion spectra in the period immediately after the arrival of a shock front (e.g., Lee 1983, Tan et al. 1986). In Fig. 4b the dashed line shows this ideal 1:1 behaviour between γ_{He} and γ_p. In this case, we find a rough agreement between predictions for a first-order Fermi process and measured data.

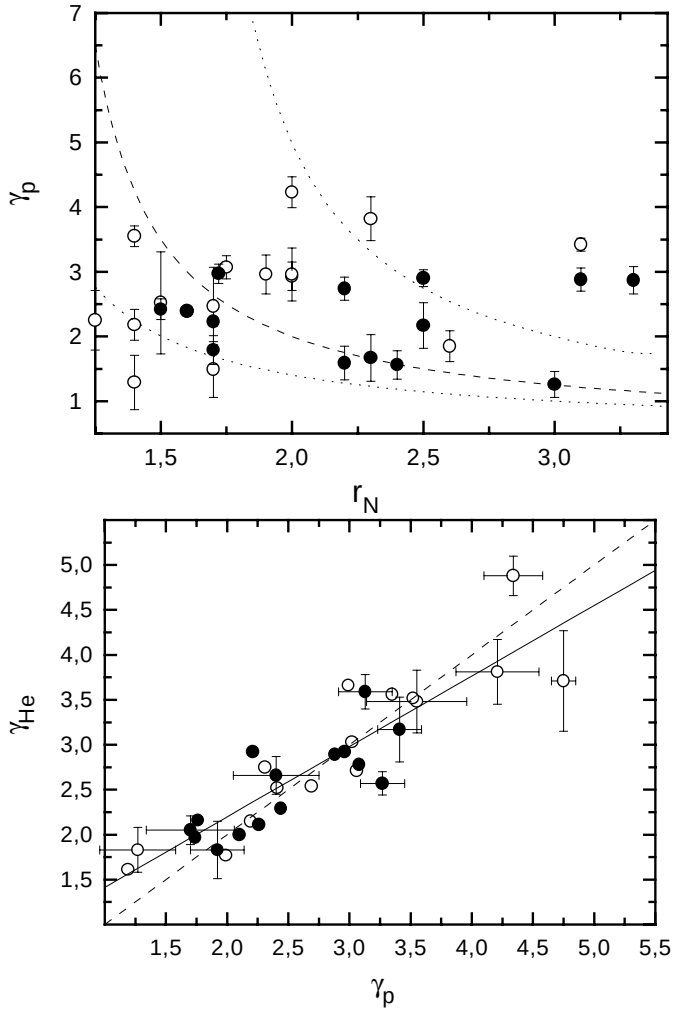

Fig. 4a and b. Correlation between the measured downstream spectral indices for protons $\gamma_{\rm p}$ and the density compression ratio r_N (**a**) and correlation between the downstream spectral indices for Helium $\gamma_{\rm He}$ and protons $\gamma_{\rm p}$ (**b**). The filled circles indicate shocks with a proton flux greater than 50 part./$({\rm cm^2 sr MeV})$. The dashed curve in **a** shows the relation $\gamma_{1st} = (r_N + 2)/(2r_N - 2)$ predicted by the first-order Fermi process. Points within the dotted lines are considered to follow the relation with a uncertainty of 30%. The solid and dashed lines in **b** represent the best linear fit for all measured spectral indices (correlation coefficient $r = 0.89$) and the expectations for a first-order Fermi process.

Looking for typical indications of particle acceleration by shock-drift acceleration we are confronted with the difficulty that this mechanism leads to no simple mathematical description of spectral indices and the relations between the indices of different ion species. Thus, we started with a search for more qualitative features of shock-drift effects, i.e., strong upstream anisotropies directed along the magnetic field, downstream anisotropies peaked more perpendicular to the magnetic field (e.g., Armstrong et al. 1985), and the occurrence of so-called shock-spike events (e.g., Decker 1988). The latter are described as extremely narrow and impulsive flux increases with a typical duration in the order of 30–60 minutes and a peak flux enhancement of roughly 2–10 for 1 MeV protons. Taking these characteristics as an evidence for shock-drift acceleration we found that at nearly all CIR related-shocks the protons showed the typical anisotropies. On the other hand only 6 shocks ($3{\rm R}_1$, 5F, 5R, 6F, 6R, and 8F) showed shock-spikes. Here, it should be mentioned that the single encounter form of shock-drift acceleration is most sufficient for quasi-perpendicular shocks. From this point of view the shock 6F with $\theta_{Bn} = 82°$ is a typical candidate for this kind of acceleration. On the other hand it is very surprising that the shock 8F with $\theta_{Bn} = 25°$ also showed shock-spikes.

4. Discussion

In the first part of our data analysis the CIR-related shocks were treated as oblique MHD shocks obeying the Rankine-Hugoniot conditions as expression of certain conservation laws in a one-fluid description. We showed that the theoretical Mach number needed for a reproduction of the measured density and magnetic field jump agrees with the measured Mach numbers within reasonable limits.

As a further test for the validity of the one-fluid picture we can use a relation between the temperature, density and magnetic field jump provided by the Rankine-Hugoniot conditions, i.e.,

$$r_T = 1 + \frac{(\kappa - 1)m_{A1}^2}{\kappa\beta_1}[1 - \frac{r_B^2}{r_N^2}]\,. \qquad (8)$$

From this it follows that for oblique MHD shocks the jump in the magnetic field strength must be smaller than the density jump because of $r_T > 1$ (entropy enhancement). For most of the shocks from Table 1 this relation holds within the given error ranges. A more detailed inspection shows that the temperature jumps computed according to Eq. 8 agree with the measured ones for roughly 80% of the shocks under consideration.

Concerning the efficiency of particle acceleration, we found that the shocks with the highest fluxes of accelerated particles seem to be supercritical shocks. Dealing with CIR-related shock waves, the reasons for this statement are twofold. First, we found that the reverse shocks are more efficient particle accelerators than the forward shocks and that the reverse shocks are moving faster than the forward ones (see Table 1). This indicates the existence of a certain threshold velocity ordering the acceleration efficiency. Secondly, we computed the magnetic field jump for critical shock waves and showed that the shock waves with the highest fluxes of high energy particles are very likely supercritcal shocks. This holds as well for 0.8–1.0 MeV protons (see Fig. 1) as for 0.1–0.4 MeV electrons (see Table 1). The exceptions are mostly related to CIR shocks with preceding travelling shocks or solar particle events. Furthermore, we can specify the conditions for efficient particle accelerating shocks. We found a critical shock velocity and a critical range for the angle θ_{Bn} (see Fig. 3). Dealing with populations of high energy electrons at CIR shocks the situation seems to be less stringent. Looking at Fig. 3 we find that high energy electrons are also observed for slowly moving or quasi-parallel CIR shocks. This situation

might be illuminated by the fact that the peak fluxes 15R, 4F, and 1F are related to CIR shocks which are preceded by travelling interplanetary shocks or by strong solar energetic particle events. So, these events might provide pre-accelerated electrons to the acceleration processes acting at the CIR shocks. Some possible acceleration processes of electrons acting at supercritical, quasi-parallel shock waves with high magnetic field turbulence were recently discussed in Mann & Claßen (1995) and Claßen & Mann (1997). In these two papers we introduced mechanisms leading to electron populations in the 10 keV energy range which could also supply the shocks with pre-accelerated electrons injected into a diffusive shock acceleration process. In order to get more information about these acceleration processes one needs spectra of the low energy electrons in the vicinity of shocks in connection with observations of the magnetic field behaviour.

Some investigations at travelling interplanetary shocks also suggest that the most efficient particle accelerating shocks are supercritical ones (e.g., Bavassano-Cattaneo et al. 1986, Lopate 1989). Both papers include measurements of the magnetic field turbulence and showed that this turbulence plays an essential role for particle acceleration. Thus, Lopate (1989) showed that three conditions are necessary for efficient electron and proton acceleration: a precursor wave in the magnetic field, a density compression ratio of $r_N > 3$, and converging scatter centers with $|\Delta V| > 50$ km/s. Since supercritical shocks are connected with a higher magnetic field turbulence and also impose a certain threshold on the density jump it seems likely to assume that high fluxes of accelerated particles were observed at supercritical shocks.

On the other hand, the data analysis in the previous section showed some differences between CIR-related and travelling interplanetary shocks. The investigations of van Nes et al. (1984) dealing with particle spectra observed at travelling shocks showed that the highest peak fluxes were observed at shocks with $30^\circ < \theta_{Bn} < 60^\circ$ while CIR shocks seem to be most efficient for $50^\circ < \theta_{Bn} < 75^\circ$. This result is also important if we discuss possible acceleration mechanisms. At the present stage we have to focus our analysis on protons and Helium with respect to their spectral indices which are available over a range of roughly 0.5–1.5 MeV/nucleon.

Here, our data analysis showed some indications of a first-order Fermi process accelerating protons and Helium, although such a process is normally assumed to act at quasi-parallel shock waves with $0^\circ < \theta_{Bn} < 45^\circ$ and most of the one- and two-dimensional hybrid simulations of shock waves show no significant acceleration of thermal ions for $\theta_{Bn} > 60^\circ$ (Baring et al. 1997). This difficulty might be surmounted taking into account, firstly, the role of interstellar pickup ions as seed particles injected into the acceleration process and, secondly, a cross-field diffusion in the downstream region. For both corrections there are observational as well as theoretical reasons. From the observational point of view it is remarkable that the proton/Helium ratio shows systematic differences between the forward and the reserve shocks; i.e., p/He at forward shocks is generally higher than p/He at reverse shocks (see Table 1). This change in the p/He ratio can possibly be explained by an acceleration of pickup helium at the reverse shock (Simnett et al. 1995). Observational evidence for cross-field diffusion at CIR shocks are the recent investigations of Dwyer et al. (1997). From the theoretical point of view these results are of great importance since cross-field diffusion is essential for allowing downstream particles to recross the shock, leading to a rapid acceleration of ions at quasi-perpendicular shocks (Jokipii 1982, 1987).

A detailed study of diffusive shock acceleration acting at CIR shock-pairs was carried out by Fisk & Lee (1980). Taking adiabatic deceleration processes into account they showed that the simple power law distribution $j(E) \propto E^{-\gamma_{1\mathrm{st}}}$ predicted by first-order Fermi processes is modified by a power law dependence in the particle velocity v and other weaker dependencies on v and the radial distance r of the CIR. A check of these predictions requires detailed fitting procedures to the observed spectra (power law or exponential spectra etc.) which are beyond the scope of the present paper, because of the limited energy range of our data. On the other hand the data in Table 1 show that the spectra observed at forward shocks are in general weaker than the spectra observed at the reverse shocks as predicted by the Fisk & Lee theory.

A comparison of the proton and Helium spectral indices with shock-drift acceleration models is complicated by the fact that shock-drift models do not readily predict spectral features. On the other hand we found indications for at least a partial influence of shock-drift effects on the populations of high energy particles, i.e., typical anisotropies and shock-spikes. Thus, the investigations of Tsurutani et al. (1982) point in a similar direction. Analysing energetic protons (1 MeV-range) observed at corotating shocks by Pioneer 10 and 11 these authors measured large field proton anisotropies and concluded that shock-drift acceleration is the primary source of these protons.

At the present stage, we can close this discussion by developing the following scenario for the ion acceleration. The acceleration process contains elements of both shock-drift and diffusion effects to enable multiple shock encounters. From this point of view the investigations of Decker & Vlahos (1986) are worth mentioning. These authors studied ion acceleration through drift *and* diffusion effects at oblique shock waves. As a special result of their test particle calculations at a shock with $\theta_{Bn} = 60^\circ$ and $r_N = 3.6$ they found a spectral index of $\gamma = 2.6$ for the energy range between 80 keV and 800 keV. This values agree roughly with the results of our data analysis for the shocks labeled 2R, 6F, and 7F. In order to generate this kind of spectra Decker and Vlahos included transverse MHD-waves in the shock vicinity. The importance of these waves lies in the fact that particle scattering at these structures enables multiple shock encounters, i.e., a typical feature of first-order Fermi, which are not included in the simple form of shock-drift acceleration.

Thus, the ions experience an acceleration process in which both shock-drift and first-order Fermi effects are closely coupled. This combination is controlled by the level of magnetic turbulence and/or the presence of suitable waves types in the shock vicinity. As a first measure for the magnetic turbulence we can take the differentiation between super- and subcritical shock waves. From this point of view it becomes clear that supercritical

shocks are more efficient in accelerating particles. Furthermore, the observation of transerve MHD-waves in quasi-perpendicular shocks only up to $\theta_{Bn} \leq 75^\circ$ (Tsurutani et al. 1983) hints at a decrease in the acceleration efficiency for nearly perpendicular shocks. A definite test of this statement requires a larger ensemble of CIR shocks. Further tests of our scenario can be obtained studying the magnetic field behaviour in the shock vicinity in high time resolution on one hand and to investigate the spectra of injected and accelerated particles in a broad energy range on the other hand. Additional information can be obtained by analysing the particle spectra (including anisotropies) as a function of the distance upstream from the shock.

5. Summary

We analysed CIR-related forward and reverse shocks experienced by the Ulysses spacecraft during its southbound journey out of the ecliptic. These shocks were treated as oblique MHD shocks with the aim to search for relations between MHD relevant parameters and the particle acceleration efficiency.

First, we computed the MHD Alfven-Mach number leading to the best fit of the density and the magnetic field jump and compared this Mach number with the measured one. The difference between these two numbers kept within reasonable limits; i.e., roughly 75% of the computed Alfven-Mach numbers are consistent with the measured ones within the computed error ranges. A further test - an explicit relation between the measured jumps in density, magnetic and temperature (Eq. 8) - confirmed this result. The data analysis showed that the forward shocks expand with a smaller velocity than the reverse shock of the same CIR. The investigation of the magnetic field jump yielded that most of the forward are subcritical while supercritical shocks are mainly found among the reverse shocks. Especially, those shocks with high fluxes of energetic particles seem to be supercritical shocks.

A more detailed analysis of the fluxes of 100–400 keV electrons and 0.8–1.0 MeV protons at the time of shock crossing confirmed the existence of critical MHD parameters for efficient particle acceleration. Although we found no simple correlation between particle acceleration efficiency and single MHD parameters (Fig. 2), it becomes clear from Fig. 3 that the shocks with the highest particles fluxes simultanously fulfill two conditions. The Alfven-Mach number M_{A1} is greater than 2.5 and the angle between the upstream magnetic field and the shock normal θ_{Bn} lies in the range 50°–75°. This result differs from simular investigations at travelling interplanetary shocks where the highest fluxes were observed within an angular range between 30° and 60° (van Nes et al. 1984).

In a further step, we discussed possible acceleration mechanisms. Here, it seems reasonable to assume that the ions are accelerated by an intimate coupling of shock-drift effects in combination with scattering processes at magnetic irregularities and/or waves in the up- and downstream region. This combination helps us to understand the higher acceleration efficiency at supercritical shocks (higher degree of turbulence) and a possibly decreasing acceleration efficiency for shocks with $\theta_{Bn} \geq 75^\circ$ (lack of upstream waves). Furthermore, there are hints for interstellar pickup ions as seed particles injected into the acceleration process.

While the high energy protons producing shocks lie in a rather restricted area this restriction is less severe for electrons. As a possible explanation, we discussed the role of electrons injected into the acceleration process from travelling interplanetary shocks and solar flare events. At the present stage of investigation the nature of the explicit electron acceleration process must remain an open question. The needs for an improved description and understanding of particle acceleration at CIR-related shocks seem to be based on investigations of the magnetic field turbulence and wave spectrum and in a detailed knowledge of the spectra of injected and accelerated particles.

Acknowledgements. We have used the solar wind plasma data, courtesy S.J. Bame, and magnetic field data from the Ulysses magnetometer, courtesy A. Balogh. We thank M.K. Reuss, R. Seidel and U. Lauth for the help in preparing the data and the stimulating discussions. The research of H.-T. C. was supported by DARA under grant no. 50 ON 9601 0.

References

Armstrong T.P., Pesses M.E., Decker R.B., 1985, in Tsurutani B.T., Stone R.G. (eds.) Collisionless Shocks in the Heliosphere: Reviews of Current Research, AGU GN-35, Washington DC, p. 271
Axford W.I., Leer E., Skadron G., 1977, Proc. 15th Int. Cosmic Ray Conf., 11, 132
Balogh A., Gonzales-Esparza, Forsyth R.J., Burton M.E., Goldstein B.E., Smith E.J., Bame S.J., 1995, Sp.Sci.Rev., 72, 171
Balogh A., Beek T.J., Forsyth R.J., Hedgecock P.C., Marquedant R.J., Smith E.J., Southwood D.J., Tsurutani B.T., 1992, A&AS, 92, 221
Bame S.J., McComas D.J., Barraclough B.L., Phillips J.L., Sofaly K.J., Chaves J.C., Goldstein B.E., Sakurai R.K., 1992, A&AS, 92, 237
Bame S.J., Goldstein B.E., Gosling J.T., Harvey J.W., McComas D.J., Neugebauer M., Phillips J.L., 1993, Geophys.Res.Lett., 20, 2323
Baring M.G., Ogilvie K.W., Ellison D.C., Forsyth R.F., 1997, ApJ, 476, 889
Bavassano-Cattaneo M.B., Tsurutani B.T., Smith E.J., 1986, J.Geophys.Res., 91, 11929
Blandford R.D., Ostricker J.P., 1978, ApJLett., 221, L29
Claßen H.-T., Mann G., 1997, A&A, 322, 696
Decker R.B., Vlahos L., 1986, J.Geophys.Res., 91, 13,349
Decker R.B., 1988, Sp.Sc.Rev., 48, 193
de Hoffmann F., Teller E., 1950, Phys.Rev., 80, 692
Dwyer et al., 1997, 2nd CIR Workshop, Elmau
Edmiston J.P., Kennel C.F., 1984, J. Plasma Phys., 32, 411
Ellison D.C., Möbius E., Paschmann G., 1990, ApJ, 352, 376
Fermi E., 1949, Phys.Rev., 75, 1169
Fisk L.A., Lee M.A., 1980, ApJ., 237, 620
Gosling J.T., 1996, ARA&A, 34, 35
Gosling J.T., Hundhausen A.J., Bame S.J., 1976, J.Geophys.Res., 81, 2111
Hundhausen A.J., 1972, Coronal expansion and solar wind, Springer, Berlin
Jokipii R.J., 1982, ApJ, 255, 716
Jokipii R.J., 1987, ApJ, 313, 842
Kantrowitz A.R., Petschek H.E., 1966, MHD characteristics and shock waves, in Kunkel W.B. (eds.), Plasma Physics in Theory and Application, McGraw-Hill, New York

Kennel C.F., Edmiston J.P., Hada T., 1985, in Stone R.G., Tsurutani B.T. (eds.) Collisionless Shocks in the Heliosphere: A Tutorial Review, AGU GN-34, Washington DC, p. 1
Keppler E., Blake J.B., Hovestadt D., Korth A., Quenby J., Umlauft G., Woch J., 1992, A&AS, 92, 317
Landau L.D., Lifshitz E.M., 1957, Electrodynamics of continua media, Fistmatgis, Moscow
Lee M.A., 1983, J.Geophys.Res., 88, 6109
Lopate C., 1989, J.Geophys.Res., 94, 9995
Mann G., Claßen H.-T., 1995, A&A, 304, 576
Mellot M.M., 1985, in Tsurutani B.T., Stone R.G. (eds.) Collisionless Shocks in the Heliosphere: Reviews of Current Research, AGU GN-35, Washington DC, p. 131
Parker E.N., 1961, ApJ, 133, 1014
Priest E., 1982, Solar Magnetohydrodynamics, Reidel, Dordrecht, NL
Russell C.T., Gosling J.T., Zwickl R.D., Smith E.J., 1983, J.Geophys.Res., 88, 9941
Russell C.T., 1985, in Tsurutani B.T., Stone R.G. (eds.) Collisionless Shocks in the Heliosphere: Reviews of Current Research, AGU GN-35, Washington DC, p. 109
Scholer M., 1985, in Tsurutani B.T., Stone R.G. (eds.) Collisionless Shocks in the Heliosphere: Reviews of Current Research, AGU GN-35, Washington DC, p. 287
Simnett G.M., Sayle K.A., Roelof E.C., 1995, Geophys.Res.Lett., 22, 3365
Smith E.J., Wolfe J.H., 1976, Geophys.Res.Lett., 3, 137
Tan L.C., Mason G.M., Ipavich F.M., Gloeckler G., 1986, J.Geophys.Res., 91, 11009
Tidman D.A., Krall N.A., 1971, Shock Waves in Collisionless Plasmas, Wiley-Interscience, New York
Tsurutani B.T., Smith E.J., Pyle K.R., Simpson J.A., 1982, J.Geophys.Res., 87, 7389
Tsurutani B.T., Smith E.J., Jones D.E., 1983, J.Geophys.Res., 88, 5645
van Nes P., Reinhard R., Sanderson T.R., Wenzel K.P., Zwickl R.D., 1984, J.Geophys.Res., 89, 2122